Available online at www.sciencedirect.com
SCIENCE DIRECT®
Finite Elements in Analysis and Design 42 (2006) 1097–1111
FINITE ELEMENTS IN ANALYSIS AND DESIGN
www.elsevier.com/locate/finel

Artificial kinematics and simple stabilization of solid-shell elements occurring in highly constrained situations and applications in composite sheet forming simulation

M. Harnau, K. Schweizerhof*

Institute for Mechanics, University Karlsruhe, 76128 Karlsruhe, Germany

Received 27 April 2005; received in revised form 10 April 2006; accepted 18 April 2006
Available online 14 June 2006

Abstract

Well-known problems which occur for mixed or underintegrated element formulations are artificial kinematics resp. numerical instabilities. These problems are also observed for 3D-shell elements as the so-called solid-shell elements especially when the loading leads to a homogeneous stress state. To prevent the elements from artificial kinematical failure a simple procedure is applied which allows to identify critical states. Then the non-necessary element modifications responsible for the numerical instabilities can be taken out.

A special application for the solid-shell elements which includes strong constraining are sheet forming problems with high stretching and large local contact pressure especially for layered composite sheets which cannot be modeled with standard 2D-shells. In the second part some numerical examples for the simulation of the forming process for pasted composite sheets are shown.

Keywords: Higher order solid-shell elements; Large deformations; Augmented Lagrangian method; Contact problems; Numerical instabilities; Sheet metal forming; Pasted composite sheets

1. Introduction

The so-called solid-shell formulation as described in [1] and e.g. [2,3] is based solely on displacement degrees of freedom belonging to the upper and lower shell surfaces and thus the use of rotational degrees of freedom can be avoided. As no kinematical assumption is applied beyond standard 3D continuum theory, general three-dimensional material laws can also be provided. In particular shell type problems with high stresses in thickness direction and considerable thinning due to stretching can be analyzed without further assumptions. Furthermore, to achieve a better geometric approximation beyond solid-shell elements with bilinear in-plane shape functions also biquadratic in-plane shape functions are considered. To overcome the locking problems, which appear for both orders of interpolation, different schemes are used and finally as proposed for example in [4] almost locking free element formulations can be derived. Only a short introduction into the solid-shell concept is also given; for further information we refer to [1,4–6] resp. [7]. A rigorous discussion and extension to multilayer problems and dynamics and a critical view on the state of art is given in [8,9]; a particular focus on large deformations and large strains is presented in [10,11].

For the forming simulation of pasted composite sheets which is discussed as a special application for the solid-shells in this contribution large deformation contact algorithms are needed. For the presented numerical examples the penalty and the augmented Lagrangian method are used for contact formulation. On the 'slave'-side, the surface of the shell structure, the contact condition is checked on the element level of so-called surface contact segments. The description of the 'master'-surfaces which are the rigid forming tools in this case is done using analytical form functions. This leads to a very efficient contact formulation but is also restricted to fairly simple contact geometries. For a detailed discussion of the used contact algorithms we refer to [7,12].

* Corresponding author. Tel.: +49 721 6082070; fax: +49 721 6087990.
E-mail address: ks@ifm.uni-karlsruhe.de (K. Schweizerhof)
URL: http://www.ifm.uni-karlsruhe.de

0168-874X/$ - see front matter © 2006 Elsevier B.V. All rights reserved.
doi:10.1016/j.finel.2006.04.003

A main focus in this contribution is on numerical defects as artificial kinematics which occur in the large deformation regime as first found by Wriggers and Reese [13]. Such numerical instabilities are due to the element modification beyond the underlying displacement formulation. With these modifications as underintegration or mixed formulation the stiffness of single eigenmodes is influenced in order to avoid locking phenomena. In cases where the specific locking effect does not occur the modification may lead to artificial kinematics, in particular under large loading, see e.g. [5]. Therefore, it should be a goal to identify the actual loading state and switch specific element modifications on or off. Such problems and the corresponding control procedures are discussed in detail in the main part of the paper. We have to note, however, that such kinematics are very similar to spurious (hourglass) modes encountered with reduced integration.

The final part of the paper deals with the forming simulation of pasted composite sheets, where very often highly constrained situations occur. The layered structure of the composite sheets is discretized with one or more solid-shell elements for each layer in the thickness direction. It can be shown that such special applications with strongly varying material and geometrical properties in the single layers of the composite sheets can be treated correctly with the introduced finite element formulations. This may be particularly important for the correct computation of eigenfrequencies of such composite sheets which are mainly used for acoustic purposes.

2. The solid-shell concept

In this section the basic features of the solid-shell concept are briefly reviewed. For a detailed explanation we refer to [1] resp. [2,3,14–17] for similar elements. A large number of so-called EAS solid-shell elements have been developed by [18–20]. Recent developments concerning a very efficient solid-shell element are given in [21]. Two different types of solid-shells have been developed within our projects (Fig. 1), the bilinear element type with four nodes on the upper and lower shell surface each and the biquadratic element type with nine in-plane nodal points on each surface. From the discrete nodal coordinates and displacements the geometry as well as the displacement field

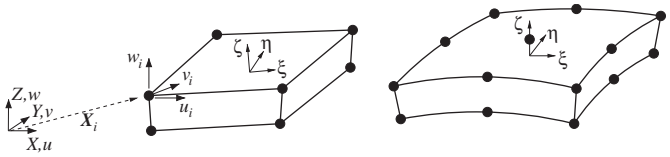

Fig. 1. Solid-shell elements with bilinear and biquadratic shapes.

are approximated using the bilinear resp. biquadratic Lagrange shape functions for in-plane approximation and a linear interpolation in thickness direction. For an extensive discussion of the solid-shell concept concerning multilayer materials we refer to [8,9] and for large strains and deformations also including dynamic loading to [10,11].

As is well known the solid-shell elements suffer from many locking effects. To avoid locking, methods of underintegrating the volume integrals [6] as well as mixed formulations (EAS-method [22] and the ANS interpolation [23,24]) are applicable. A complete discussion about these locking phenomena and different developed element versions is given e.g. in [4] and more recently in [18–20]. Finally, almost locking free 3D-shell elements are available. The nomenclature for the element versions relevant for the investigations in the following chapters is given in Table 1. All elements but the displacement elements (DIS) contain an assumed transverse shear strain interpolation [23,24]. Another modification applied to all elements is the thickness strain enhancement as proposed by [25] denoted by (...EAS) at the end of the chosen names. The final modification is concerning the membrane strains, where an enhancement by four terms (EAS...) or by six terms (eas...) is used for the elements with bilinear interpolation in in-plane direction. For elements with biquadratic in-plane interpolation an assumed strain interpolation is used in in-plane direction following the proposal of Bathe and Bucalem [24] and is thus denoted with (MI9K...).

The use of nonlinear material laws, necessary for the treatment of large deformation problems, is described in detail e.g. in [6,26]. It should be mentioned that in contrast to the degenerated shell concept strains and stresses in thickness direction are included in the solid-shell concept, thus general three-dimensional material laws can be used without

Table 1
Nomenclature for solid-shell element formulations based on the introduced modifications; linear interpolation in thickness direction

Element name	In-plane approximation	Membrane strain modification	Thickness strain modification	Transverse shear strain modification
DIS3D	Bilinear Lagr.	–	–	–
DIS3DEAS	Bilinear Lagr.	–	EAS	–
ANS3DEAS	Bilinear Lagr.	–	EAS	ANS
EAS3DEAS	Bilinear Lagr.	EAS (4 param.)	EAS	ANS
eas3DEAS	Bilinear Lagr.	EAS (6 param.)	EAS	ANS
MI9K3DEAS	Biquadratic Lagr.	ANS	EAS	ANS
...-rv	Selective reduced integration of volumetric terms			
...-ri	Reduced integration of all terms			

DIS is the displacement element, ANS is assumed natural strain interpolation, EAS is enhanced strain interpolation.

any modification and general 3D stress and strain states can be treated directly.

3. Artificial element kinematics for solid-shell elements with mixed interpolation

By using methods of underintegration and mixed element formulations the approximations within an element concerning strains are modified and finally locking free element formulations can be provided. However, the modifications can also lead to artificial singularities in the element stiffness matrix, so-called numerical instabilities. This behavior can also be shown in analytical investigations e.g. in [5,13]. From these investigations we find that this behavior has to be expected mainly for homogeneous stress states, for other non-homogeneous cases we refer to [27]. For such states a locking free result can also be achieved using the pure displacement element which is also free of artificial kinematics. Thus a possible solution to avoid numerical instabilities is to identify homogeneous stress states and then switch off the corresponding non-required element modifications. A similar procedure has been suggested by Wall et al. [28] where the mixed functional is modified with some self-adjusting factors for homogeneous stress states to avoid kinematics. Further mixed element formulations which are free of artificial kinematics in large deformations have been developed by Glaser and Armero [26] and Korelc and Wriggers [29] where local instabilities are detected by eigenvalue analysis and removed for some specific nonlinear materials and a specific example. Reese [30–32] uses a stabilized formulation, which allows to find local element instabilities and to remove them within the stabilization procedure involved in the element derivation. A further advantage is a high distortion insensitivity of the element, as one-point integration is used. However, also an eigenvalue analysis is necessary on element level.

It is rather surprising that beyond [5] there is little information on artificial kinematics for solid shell elements throughout the literature, which may be due to the fact that so-called constrained situations leading to such kinematics are not very often encountered. Further we have to note at this point that stabilization is by no means a new idea, as spurious modes are typically encountered with reduced integration. For such spurious modes sophisticated filtering or stabilization methods have been proposed since long e.g. by Vu Quoc and coauthors [33,34]. Two other stabilization schemes which are fairly simple but may not work in all cases are the so-called viscous and stiffness hourglass controls found in most commercial explicit FE programs.

However, the scheme proposed in the following section is not intended to filter out modes or check for these modes directly and stabilize them in one or the other way. We rather aim at a so-called 'smart' element and propose to remove the corresponding 'responsible' modification based on a detection scheme. The wording 'stabilization' is then a slight misuse compared to the other mentioned stabilization techniques.

3.1. Simple stabilization by switching off critical element modifications

The pure displacement solid-shell element can perfectly represent homogeneous stress states and shows no numerical instabilities for such homogeneous stress states which are critical for the modified elements. Therefore such 'critical states' should be identified and the non-required element modifications should be switched off, which leads to a so-called 'smart' element. To decide which modification is required and which is not the internal energy of each element is determined for the modified as well as the unmodified element, the pure displacement version. For the latter element the internal energy is computed using the strain tensor which is compatible with the displacement approximation

$$\boldsymbol{E}_{\mathrm{dis}} = \boldsymbol{E}(\boldsymbol{u}). \tag{1}$$

For element formulations with modified strains according to either the ANS- or to the EAS-method the strain tensor is computed as

$$\boldsymbol{E}_{\mathrm{mod}} = (\boldsymbol{E}_{\mathrm{dis}})_{\mathrm{ANS}} + \boldsymbol{E}_{\mathrm{EAS}}. \tag{2}$$

In both cases the internal energies are computed as

$$\Pi_{\mathrm{dis}} = \int_V \boldsymbol{E}_{\mathrm{dis}}^{\mathrm{T}} \boldsymbol{S}_{\mathrm{dis}}\, \mathrm{d}V, \quad \Pi_{\mathrm{mod}} = \int_V \boldsymbol{E}_{\mathrm{mod}}^{\mathrm{T}} \boldsymbol{S}_{\mathrm{mod}}\, \mathrm{d}V. \tag{3}$$

For Π_{mod} also a selective reduced integration of the volumetric parts can be applied.

Both energy values Π_{mod} and Π_{dis} are necessary for a proper identification of the stress state. If $\Pi_{\mathrm{mod}} < \Pi_{\mathrm{dis}}$, locking has to be expected. Then the corresponding modification has to be included. For a homogeneous stress state $\Pi_{\mathrm{dis}} = \Pi_{\mathrm{mod}}$ is obtained, then the pure displacement formulation is used.

The various element modifications are associated with different locking phenomena and should be treated separately. Therefore when computing Π_{mod} the single modifications have to be taken into account separately

Π^1_{mod} ... Only assumed strains (ANS) for the transverse shear strains,
Π^2_{mod} ... Only enhanced strains (EAS) for $E_{\zeta\zeta}$,
Π^3_{mod} ... Only EAS (bilinear elements) or ANS (biquadratic elements) for the membrane strains,
Π^4_{mod} ... Only selective reduced integration of the volumetric parts (-rv).

If the ratio $(\Pi_{\mathrm{dis}} - \Pi^n_{\mathrm{mod}})/\Pi_{\mathrm{dis}},\ n = 1, \ldots, 4$ becomes smaller than a certain tolerance *tol* for each of the n considered cases then the according modification appears to have no influence on the element behavior. As a consequence, the corresponding modification can be left out and then the corresponding numerical instabilities cannot be excited. Within the numerical examples $tol \approx 0.01$ is chosen which seems to be working very well. If such a stabilization is applied we denote it by adding $(..)_{\mathrm{stab}}$ to the name of the element.

Thus the stabilization is primarily based on the computation of the strain energy ratios $(\Pi_{\mathrm{dis}} - \Pi^n_{\mathrm{mod}})/\Pi_{\mathrm{dis}}$ for all the

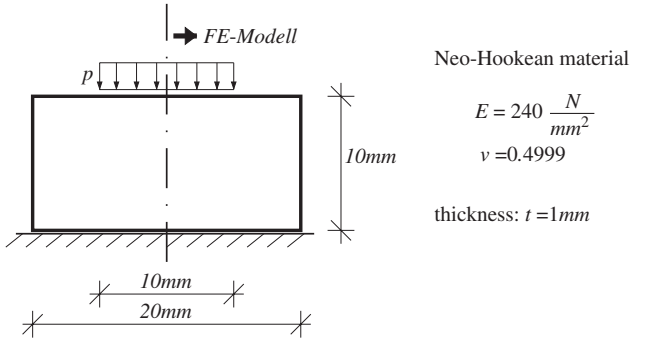

Fig. 2. Slab loaded by line load for inhomogeneous compression test; geometry, material properties and boundary conditions.

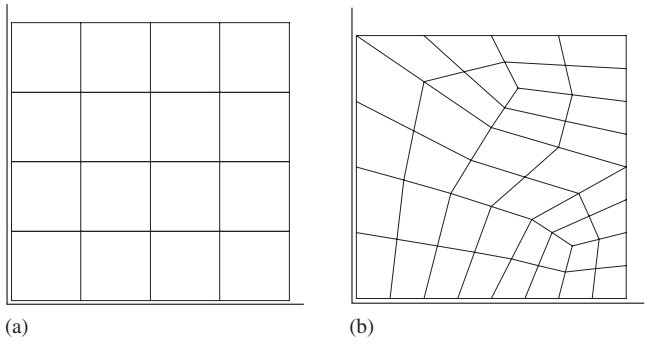

Fig. 3. FE-discretization of slab—considering symmetry—for inhomogeneous compression test: (a) uniform coarse mesh; (b) distorted fine mesh.

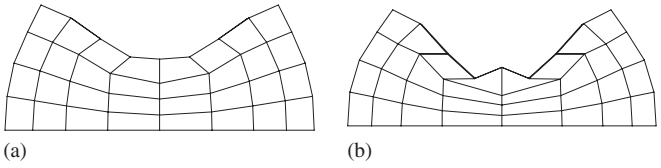

Fig. 4. Deformed slab (uniform coarse mesh); center compression of (a) 40% and (b) 46%; unstabilized EAS3DEAS element.

available element modifications. Then the decision follows which of the modifications has to be left out or considered. This can be done e.g. after every iteration or after every load step. In general, the energy values could be determined even with larger intervals.

The check of the strain energy ratios seems to be a very simple and efficient way to decide if one element modification could lead to an artificial numerical instability. Of course the success of this algorithm depends on the choice of the tolerance values and it also has to be decided where and how often the check is done. Alternatively an eigenvalue analyses of the tangent stiffness could also be performed with the disadvantage that if zero eigenvalues occur it cannot be easily decided which element modification is responsible for the numerical instability. The strain energy ratios also seem to be a good indicator to detect numerical instabilities before they really appear. If a critical case cannot be detected in advance, the algorithm has to be modified in such a way that if a numerical instability is detected the equilibrium iteration is not continued but again started from the beginning of the actual load step with the responsible element modification taken out.

3.2. Inhomogeneous compression test

The simple stabilization proposed in the previous section is tested numerically performing an inhomogeneous compression test. For homogeneous compression the procedure should always lead to a proper result because then Π_{dis} is almost identical to Π_{mod} and therefore the pure displacement formulation would be automatically used. In the inhomogeneous compression case locking as well as artificial kinematics due to parts with almost homogeneous stress states can appear. This test has been suggested originally in [30,35], for further analyses see [31,32].

A rectangular slab with thickness t is partially loaded inplane by a line load p (see Fig. 2). The material behavior can be described using a Neo-Hookean material model with the parameters suggested in [30,35], thus the shear modulus is computed based on Young's modulus and the given Poisson ratio. Due to symmetry only half of the structure is discretized in the considered FE modeling. For the FE formulation the bilinear EAS3DEAS and the biquadratic MI9K3DEAS element with modifications of membrane, transverse shear and thickness strains are taken. The stabilized versions are based on the same element formulations with the option to take out each of the above mentioned modifications separately. In addition the selective reduced integration of the volumetric terms is considered, if indicated by the energy check. Therefore these elements are named as $(\text{EAS3DEAS-rv})_{\text{stab}}$ or $(\text{MI9K3DEAS-rv})_{\text{stab}}$.

3.2.1. Uniform coarse discretization

First the slab is discretized with a uniform mesh with 16 bilinear or four biquadratic elements thus with 5×5 nodal points (see Fig. 3a). In addition in every load step the eigenvalues of the stiffness matrix are analyzed to detect possible numerical instabilities also directly.

In Fig. 4 the deformation of the slab is depicted for the bilinear EAS3DEAS element for a center compression of 40% or 46%. From Table 2 we recognize that negative eigenvalues of the stiffness matrix are present already for a rather low load level. For a center compression of about 46% convergence of the equilibrium iterations within the solution of the nonlinear problem is no longer achieved and the analysis has to be stopped; the artificial kinematics in this case are clearly visible in Fig. 4b. As we expect some volumetric locking with the specific material also the EAS3DEAS-rv element with additional selective reduced integration of the volumetric parts is used. As expected it behaves softer as a lower loading value is necessary to reach the center compression value of 40%. The computation for this element version has to be stopped at a compression of about 58% as the convergence in the equilibrium iterations is no longer achieved.

Alternatively, the slab is discretized with four biquadratic elements. The results of this investigation are also given in

Table 2
Uniform coarse mesh; comparison of results for various element versions; deformation status and corresponding pressure loading for different compression values; occurrence of negative eigenvalues at pressure level

	40% compr. for	65% compr. for	Neg. eigv. for
	p in N/mm^2		
Q1SP in [35,30,31]	∼ 210	∼ 600	–
EAS3DEAS	214	No conv.	30
EAS3DEAS-rv	188	No conv.	–
(EAS3DEAS-rv)$_{stab}$	203	477	–
MI9K3DEAS	No conv.	–	48
MI9K3DEAS-rv	No conv.	–	–
(MI9K3DEAS-rv)$_{stab}$	228	540	–

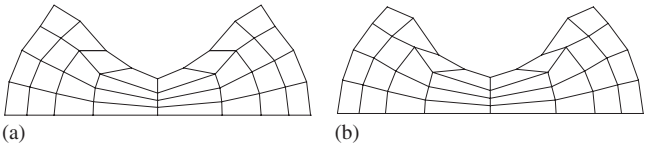

Fig. 5. Deformed slab (uniform coarse mesh); center compression of 65%; (a) (EAS3DEAS-rv)$_{stab}$ element and (b) (MI9K3DEAS-rv)$_{stab}$ element.

Table 2. In the analysis with the MI9K3DEAS element also artificial kinematics are observed which leads to divergence in the equilibrium iterations already for a compression of about 14% and a negative eigenvalue occurs already for a rather small load. For the MI9K3DEAS-rv element with selective reduced integration of volumetric terms no negative eigenvalues can be observed but the computation has to be stopped due to divergence for a compression of about 38%.

To test the proposed stabilization procedure the bilinear as well as the biquadratic element formulations with all available strain modifications and selective reduced integration of the volumetric terms are included. The modifications which are found to be responsible for the numerical instabilities are then switched off denoted by $(..)_{stab}$. In this example—as expected—the modifications concerning (i) the transverse shear strains, (ii) the enhancement of the normal strain in thickness direction and (iii) the modifications of the membrane strains are taken out for the complete mesh immediately after the stabilization is initialized for the first time. The selective reduced integration of volumetric parts is —not unexpectedly—retained for the complete mesh. The deformation for 65% compression is shown in Fig. 5. Both stabilized versions—essentially identical to selective reduced integrated elements—lead to the expected improved results.

From the analyses we can further conclude for this plane shell structure loaded in in-plane direction, that both basic elements are almost equivalent; the modified bilinear element behaves slightly softer for this fairly coarse mesh than the biquadratic elements. Both element types show a considerable deviation to the results obtained in [30,31,35] for 65% compression.

Table 3
Distorted fine mesh; comparison of results for various element versions; deformation status and corresponding pressure loading for different compression values; occurrence of negative eigenvalues at pressure level

	40% compr. for	65% compr. for	Neg. eigv. for
	p in N/mm^2		
Q1SP in [35,30,31]	∼ 210	∼ 600	–
EAS3DEAS	213	No conv.	–
EAS3DEAS-rv	No conv.	–	–
(EAS3DEAS-rv)$_{stab}$	202	505	–
MI9K3DEAS	No conv.	–	24
MI9K3DEAS-rv	No conv.	–	–
(MI9K3DEAS-rv)$_{stab}$	210	599	–

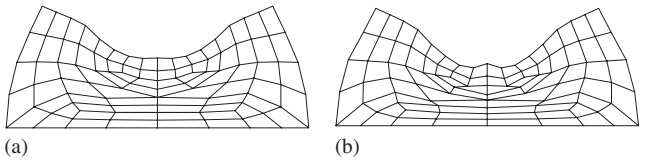

Fig. 6. Deformed slab (distorted fine mesh); center compression of (a) 40% and (b) 46%; unstabilized EAS3DEAS element.

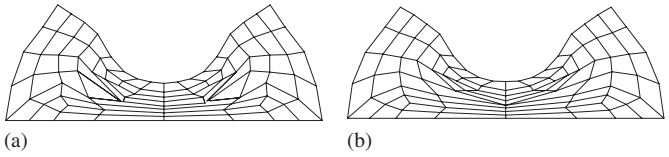

Fig. 7. Deformed slab (distorted fine mesh); center compression of 65%; (a) stabilized (EAS3DEAS-rv)$_{stab}$ element and (b) (MI9K3DEAS-rv)$_{stab}$ element.

3.2.2. Distorted fine mesh

As a second test the slab is discretized with a distorted and slightly refined mesh using 40 bilinear or 10 biquadratic elements (see Fig. 3b) based on the same 53 nodal points. For the distorted FE mesh similar results are obtained as with the uniform mesh. However, contrary to the uniform mesh no negative eigenvalue appears for the bilinear EAS element up to the considered load level (see Table 3). Nevertheless the computation has to be stopped as convergence in the equilibrium iterations could not be achieved for compression values beyond 46%. In Fig. 6 the deformed slab is depicted for compression values of 40% or 46% in the center of the slab. Apparently the in-plane modifications lead to some instabilities or artificial kinematics visible in Fig. 6b. Using the EAS3DEAS-rv element only a compression value of 36% is reached until the computation has to be stopped due to convergence problems. With the stabilized version (EAS3DEAS-rv)$_{stab}$ a result which is free of artificial kinematics is achieved (see Fig. 7a). The element modifications concerning transverse shear and normal strain in thickness direction are immediately switched off. The modifications concerning the membrane strains are partially switched off at the first time the stabilization is initialized and completely switched off at a compression value of about 60%. This element version

also delivers the softest answer which indicates that this result is almost locking free. Thus the modifications to remove volumetric locking appear to be necessary for the complete mesh.

The results for the mesh with biquadratic elements are also given in Table 3 and Fig. 7b. For the MI9K3DEAS element—almost identical as for the uniform coarse discretization—one negative eigenvalue is found already for a compression value of about 7% with $p = 24\,\mathrm{N/mm^2}$. Then no convergence in the equilibrium iterations can be achieved. For the MI9K3DEAS-rv element with selective reduced integration of the volumetric parts the computation diverges for a compression value of about 30%. An improved and stable result is obtained with the stabilized version $(\mathrm{MI9K3DEAS\text{-}rv})_{\mathrm{stab}}$, where all modifications but the volumetric reduced integration are switched off. Again the modifications concerning the transverse shear strains and the normal thickness strains are immediately switched off while the changes concerning the membrane strains are partially left until a compression value of about 60%.

Finally we can summarize that for the discretization with distorted elements only for the biquadratic MI9K3DEAS element negative eigenvalues of the stiffness matrix can be observed in the equation solving, before also convergence is no longer obtained. Looking at the loading/compression values the results for the distorted mesh are showing a clearly stiffer behavior at higher deformation states compared to the uniform mesh even though a finer discretization is used for the distorted mesh version. It is interesting that the results for the biquadratic elements are almost identical to the results found in [30,31,35] with the trilinear specifically stabilized elements and a slightly finer mesh. However, it remains questionable whether the element deformations are not too large to lead to acceptable results. Nevertheless the numerical tests have shown that the proposed procedure leads to a 'robust' analysis and correct results for the investigated problems. However, the distortion sensitivity is larger than for the stabilized elements in [30,31,35].

3.3. Numerical instabilities of ANS-elements under shear loading

The deformation process for pasted composite sheets modeled with layers of solid-shell elements (see e.g. Fig. 10) involves bending. In this case the two face sheets are also moved in opposite direction which results in pure shear loading of the core sheet. In general the discretization involves multiple solid-shell elements in the thickness direction; one for each face sheet and one or more elements for the core layer. While with one element for the core the analysis could be performed without problems, using a core layer discretization of more than one ANS-elements in thickness direction leads to artificial kinematics inside the core layer. The reason for apparent success with one element is due to the constraining of the single element by the two outer layers.

To get a better insight into this artificial kinematics the simple problem shown in Fig. 8 is investigated, where a layered structure discretized with three ANS3DEAS elements in thickness direction is loaded in in-plane direction by an imposed displacement $u = 0.02$ of all nodes at the upper surface. Thus a pure shear loading is applied. The geometry and material properties are chosen according to the parameters given in Section 4 for a standard core layer of composite sheets. As the material remains in the elastic range for this load case, the core layer materials in this section are chosen to be equivalent to an elastic neo-Hookean material. The deformed structure shown in Fig. 9 is achieved after the first solution step. In Fig. 9(a) the artificial kinematics appearing for the discretization with the ANS3DEAS elements are clearly visible. These kinematics are obviously due to the transverse shear interpolation leading to an underintegration effect. Further investigations show that this effect is caused by the chosen material properties. For the bending modes very high eigenvalues are found because of the rather high degree of incompressibility on one hand and on the other hand the very small elastic stiffness modulus together with the small thickness value of the elements leads to eigenvalues close to zero. This results in a kinematical effect due to a numerical problem. Using a Poisson's ratio of e.g. $\nu = 0.49$ for the computation leads to a more stable behavior identical as shown in Fig. 9(b).

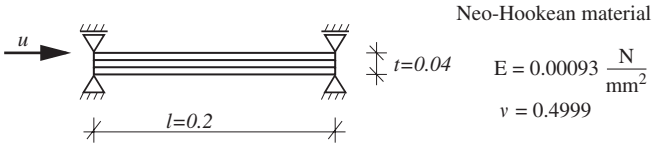

Fig. 8. Shear test with layered structure modeled with three solid-shell elements in thickness direction; geometry, material properties and boundary conditions.

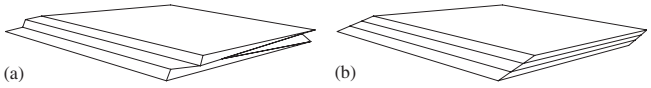

Fig. 9. Layered structure under shear loading: (a) ANS3DEAS elements and (b) $(\mathrm{ANS3DEAS})_{\mathrm{stab}}$ elements.

The ANS-modification is used to avoid locking for thin elements under bending thus the eigenvalues of some bending modes are lowered. Not using the ANS-modification for the case shown in Fig. 9, where no bending is present has some kind of stabilizing effect and these artificial kinematics can be avoided. As a consequence the computation is then performed with the pure displacement formulation. To initiate the stabilization also the modified strain energies have to be computed in order to include the modifications as needed. In this case none of the available modifications is turned on and the $(\mathrm{ANS3DEAS})_{\mathrm{stab}}$ element becomes fully equivalent to the pure displacement formulation.

Within the further investigations also the eigenvalues of the stiffness matrix of one 'composite element' are computed. A single 'composite element' consists of one element for each face layer and one or three elements for the core layer as shown in Fig. 10. The thickness for one composite element is 1.04 mm, with 0.5 mm for the face layers each and 0.04 mm

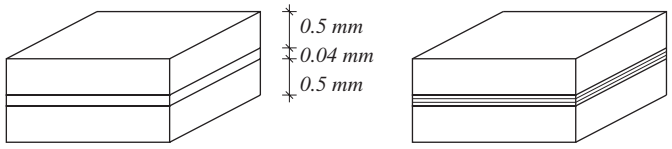

Fig. 10. Single composite 'Bondal®-element' with variations of core layer discretization.

Table 4
Material parameters for the face sheets

κ (kN/cm^2)	μ (kN/cm^2)	τ_0 (kN/cm^2)	τ_∞ (kN/cm^2)	H (kN/cm^2)	δ (–)
17,500	8077	16.5	40	20	20

Table 5
Material parameters for core layer; Bondal®N/M

κ (kN/cm^2)	μ (kN/cm^2)	τ_0 (kN/cm^2)	H (kN/cm^2)
100	0.00031	46	160

Table 6
Material parameters for core layer; Bondal®H

κ (kN/cm^2)	μ (kN/cm^2)	τ_0 (kN/cm^2)	H (kN/cm^2)
1000	0.072	6.5	28

for the core layer. For discretization of each face layer one bilinear ANS3DEAS element is used, the core layer is discretized with different variants of the solid-shell element formulation while one or three elements are used in thickness direction. The considered material properties are given in Tables 4–6 and are discussed in detail in the following sections.

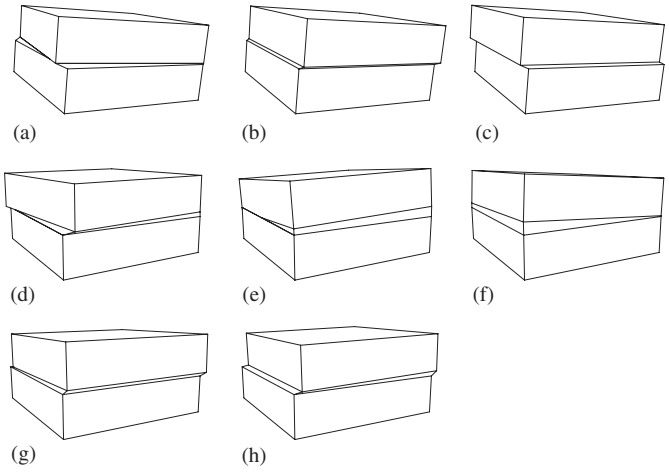

Fig. 11. Eigenmodes with corresponding eigenvalues inside the observed range for composite element; (a)–(c) ANS3DEAS(1 cl.el.); (d)–(h) DIS3D-ri, DIS3D-rv and eas3DEAS (1 cl.el.).

The results of the eigenvalue analysis of a single 'Bondal®' element are given in Table 7 where only the numbers of eigenvalues with values $EV < 10^{-1}$ or $EV < 10$ are shown. If the core layer is discretized with only one element in thickness direction using the ANS3DEAS element for the Bondal®N/M as well as for the Bondal®H three rather small eigenvalues are observed. The corresponding eigenmodes describe the shear deformation of the core layer with two translational modes and one rotational mode of the face layers against each other (see Fig. 11(a)–(c)). However, they do not indicate any element

Table 7
Eigenvalues of the initial tangential stiffness matrix for one composite element; varying core layer discretization and material properties for core layer; 1 core element 1 cl.el./3 core elements 3 cl.el.

Eigenvalues for Bondal®N/M				
Core layer element	$EV < 10^{-7}$	$10^{-7} < EV < 10^{-5}$	$10^{-5} < EV < 10^{-3}$	$10^{-3} < EV < 10^{-1}$
ANS3DEAS (1 cl.el.)	–	–	3	–
DIS3D-rv (1 cl.el.)	–	–	5	–
DIS3D-ri (1 cl.el.)	3	–	2	–
eas3DEAS (1 cl.el.)	–	–	5	–
ANS3DEAS (3 cl.el.)	–	8	5	6
DIS3D (3 cl.el.)	–	–	6	13
DIS3DEAS (3 cl.el.)	–	–	11	8
DIS3D-rv (3 cl.el.)	–	–	13	14
Eigenvalues for Bondal®H				
Core layer element	$EV < 10^{-5}$	$10^{-5} < EV < 10^{-3}$	$10^{-3} < EV < 10^{-1}$	$10^{-1} < EV < 10^{1}$
ANS3DEAS (1 cl.el.)	–	–	3	–
DIS3D-rv (1 cl.el.)	–	–	5	–
DIS3D-ri (1 cl.el.)	3	–	2	–
eas3DEAS (1 cl.el.)	–	–	3	2
ANS3DEAS (3 cl.el.)	–	8	3	8
DIS3D (3 cl.el.)	–	–	5	14
DIS3DEAS (3 cl.el.)	–	–	5	14
DIS3D-rv (3 cl.el.)	–	–	8	19

kinematics. Using the DIS3D-rv, the DIS3D-ri or the eas3DEAS element for core layer discretization five eigenvalues (see Fig. 11(d)–(h)) appear inside the observed range. This number indicates a better behavior concerning incompressibility locking, thus these combinations are preferable for the numerical examples in the following section. The three kinematic eigenvalues of the DIS3D-ri element ($EV < 10^{-3}$) do not lead to a global kinematic behavior because the core layer is constrained between the face layers.

If the core layer is discretized with three elements in thickness direction for the Bondal®N/M as well as for the Bondal®H, 19 eigenvalues for the DIS3D/DIS3DEAS elements or 27 eigenvalues for the DIS3D-rv element are obtained inside the observed range up to 10^{-1} and 10^{1}. For the discretization with ANS-elements eigenvalues much smaller than the eigenvalues for the discretization with only one core layer element are observed. The corresponding eigenmodes describe deformations inside the core layer according to the kinematics shown in Fig. 9. Leaving out the ANS-modification thus using the DIS3D-elements for the core layer the very low eigenvalues indicating kinematics can be avoided and apparently reasonable eigenvalues are obtained. The artificial kinematics can be again identified as the result of a purely numerical problem. The very small stiffness of the core layer combined with the much stiffer face layer elements lead to a high difference between the smallest and the highest eigenvalue of the stiffness matrix resulting in numerical problems when solving the global equation system. Using a higher Young's Modulus for the core layer shows that the smallest eigenvalue is also increasing while the highest eigenvalue remains unchanged thus no kinematics are observed any more. For the following computations the DIS3D-rv element is taken expecting an improved behavior concerning incompressibility locking.

For the general model we can draw the following conclusion: if the shear stiffness of the core layer should be roughly captured the discretization with only one element in thickness direction is apparently sufficient. If the deformations inside the core layer should be captured in more detail a higher number of elements in thickness direction must be used. Then the transverse shear interpolation has to be taken out to prevent numerical instabilities thus artificial kinematics inside the core layer. In order to avoid incompressibility locking appropriate elements as eas3DEAS or DIS3D-rv should be used.

4. Numerical investigation of pasted composite sheets

The following investigations are performed on practical problems where such highly constrained situations occur. This is primarily in metalforming, whereas in stability analysis of shell structures we have only little constraining thus hardly any homogeneous loading state leading to the problems discussed above. Pasted composite sheets are preferably taken for constructions to reduce acoustic noise emission. Applications for composite sheets are e.g. in mechanical engineering for machine casing or fabrication of car body parts and also in civil engineering for wall constructions. If ordinary metal sheets without any further additions are taken, often costly damping actions are necessary to fulfill requirements concerning specific vibration characteristics, whereas pasted composite sheets a priori have good vibration damping properties due to the separation by a softer layer and the interaction between the layers. Further details about applications and the description of experimental and numerical investigations can be found e.g. in [36].

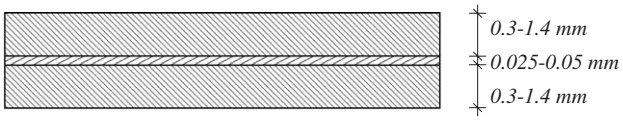

Fig. 12. Layer composition of pasted composite sheets.

In the production process of pasted composites two metal sheets of thickness 0.3–1.4 mm are glued together, therefore, the composites consist of two face sheets of the same metallic material and a glue core layer of thickness 0.025–0.05 mm (Fig. 12). For discretization of all layers of the pasted composite sheets the so-called solid-shell elements, introduced in Section 2 are used. Such shell elements are preferable for the discretization of layered structures because of their inherent 3D character.

4.1. Material properties and discretization of the composite sheets

The material properties for the face layers are described assuming elasto-plastic material behavior with a Hencky elastic strain energy function and von-Mises plasticity with isotropic hardening of saturation type. The material law taken is described in detail in [37] based on derivations by Simo [38], where for the kinematics of the deformation a multiplicative split of the deformation gradient $\boldsymbol{F} = \boldsymbol{F}^e \cdot \boldsymbol{F}^{\mathrm{p}}$ into an elastic and a plastic part is supposed. This split involves the introduction of the determinant $J^e = \det \boldsymbol{F}^e$ of the elastic deformation gradient that measures the local elastic change of volume. In spectral decompositions the principal elastic stretches λ_i^e, the isochoric principal elastic stretches $\hat{\lambda}_i^e = (J^e)^{-1/3}\lambda_i^e$ and their logarithms $\varepsilon_i^e, \hat{\varepsilon}_i^e$ are introduced as well. We further consider isotropic finite elastoplasticity with an additive split of the energy function

$$W(\varepsilon_1^e, \varepsilon_2^e, \varepsilon_3^e, \xi) = \widehat{W}(\hat{\varepsilon}_1^e, \hat{\varepsilon}_2^e, \hat{\varepsilon}_3^e) + U(J^e) + W^{\mathrm{p}}(\xi), \tag{4}$$

which consists of three parts: an isochoric elastic part $\widehat{W}$, a volumetric elastic part U and a plastic part W^{p}. The plastic part depends on the scalar internal state variable ξ (equivalent plastic strain) and represents the isotropic plastic hardening behavior of the material. The energy function W with

$$\begin{aligned} &\widehat{W} = \mu[(\hat{\varepsilon}_1^e)^2 + (\hat{\varepsilon}_2^e)^2 + (\hat{\varepsilon}_3^e)^2], \quad U = \kappa(\ln J^e)^2/2, \\ &W^{\mathrm{p}} = H\xi^2/2 + (\tau_\infty - \tau_0)\xi + \delta^{-1}(\tau_\infty - \tau_0)\exp(-\delta\xi) \\ &\text{with} \ \ \delta > 0 \end{aligned} \tag{5}$$

is taken from [38]. The elastic terms $\widehat{W}$ and U are as introduced by Hencky [39]. The plastic term W^{p} yields a saturation type hardening law. The material parameters are given in Table 4.

For the elastic range the bulk modulus κ and the shear modulus μ are computed based on Young's modulus $E = 21\,000(\mathrm{kN})/\mathrm{cm}^2$ and Poisson's ratio $\nu = 0.3$ normally used to describe the elastic behavior of steel. For the plastic range the initial yield stress τ_0 is given. The isotropic hardening of saturation type is defined by the linear hardening modulus H, the saturation yield stress τ_∞ and the saturation exponent δ.

For the core layer an elasto-plastic material law with neo-Hookean elasticity and von-Mises plasticity with linear isotropic hardening is used. As two different types of composite sheets, the Bondal®N/M[1] composite and the Bondal®H composite are investigated, two sets of material parameters for the core sheet are given in Tables 5 and 6. The computation of the material properties is described in [7] in a more detailed fashion, based on experimental results published in [36]. For further analysis and the discussion of the results we have to note, that Bondal®N/M is less stiff than Bondal®H by a factor larger than 10, but both, the yield stress and the hardening modules, are much larger for the first one.

In the numerical investigation the forming process has to be simulated followed by an eigenvalue analysis in order to investigate the vibration characteristics of the structure. Thus extensive parameter studies can be performed to optimize the components concerning the vibration characteristics.

The finite element discretization of the composite sheets in thickness direction is done using the introduced solid-shell elements with one element for the face layers each and one or more elements for the core layer. Four different element combinations

- ANS3DEAS/DIS3D-ri,
- ANS3DEAS/eas3DEAS,
- MI9K3DEAS/MI9K3DEAS-rv,
- ANS3DEAS/DIS3D-rv (three core layer elements)

three with bilinear elements and one with biquadratic elements, are chosen for the following examples. For the bilinear element model the face sheets are modeled with ANS3DEAS elements, as predominantly bending is expected for these rather stiff parts. For the core layer with nearly incompressible but soft material behavior which is primarily shear loaded first the reduced integrated displacement DIS3D-ri is tested. This element version should be free of any locking. A kinematic behavior of this element is prevented by the supporting face layer elements. Alternatively the six-parameter EAS-element version eas3DEAS, which should not show any kinematics and no volumetric locking is taken. For the biquadratic model the MI9K3DEAS element is used for the face layers in combination with the MI9K3DEAS-rv, selective reduced integration of the volumetric parts for the core layer. Finally, a core layer discretization with three elements in thickness direction is also tested. Here, as discussed in the previous section, kinematics inside the core layer may appear with the ANS-elements. Thus, by using the procedure as proposed above all critical element modifications are switched off but the selective reduced integration of the volumetric parts to avoid incompressibility locking which leads finally to the DIS3D-rv element.

[1] Bondal® is a protected label of the ThyssenKrupp Stahl AG.

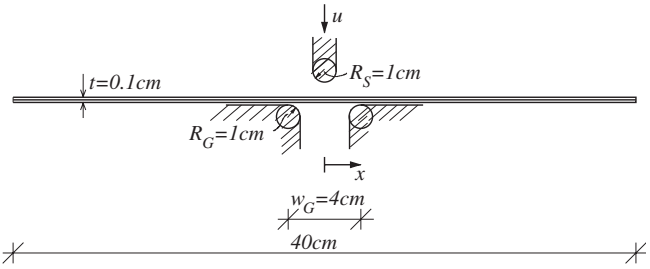

Fig. 13. Geometry properties for free bending investigation.

4.2. Free bending of a composite sheet

In this section the free bending process for a sheet with a length of 40 cm is simulated. This example is taken from the numerical and experimental investigations described in [36]; we have to note, however, that only some experimental results are depicted in [36]. The total thickness of the composite sheet is assumed as $t = 1$ mm with a thickness of 0.04 mm for the core layer with the material properties given in Section 4. In the FE model only a strip is discretized with the nodes in the out-of-plane direction all fixed; thus a plane strain state is modeled. The dead load of the structure is also taken into account.

Within the free bending process the workpiece originally resting on the die is undergoing bending by pressing the sheet with a punch against the edges of the die. The geometry data for the die and the punch are given in Fig. 13, with the width of the die as $w_\mathrm{d} = 40$ mm and the radii for the punch and the edges of the die as $R_\mathrm{p} = R_\mathrm{d} = 10$ mm.

For discretization in longitudinal x-direction 38 bilinear or 19 biquadratic elements with the same number of nodes are used and symmetry at $x = 0$ is taken into account. The sheet is discretized with a very fine mesh in the area where the punch is pressing against the sheet because a strong curvature of the deformed sheet has to be expected there. To describe the contact between the sheet and the rigid tools a pure penalty approach with a penalty parameter of $\varepsilon_\mathrm{p} = 8.0$ is used. The penetration values occurring in this analysis are very small with the chosen penalty parameter, thus an additional augmentation procedure for the contact forces as described in [12] for the so-called augmented Lagrangian approach is not necessary.

The deformed meshes for Bondal®N/M and Bondal®H are shown in Figs. 14 and 15 for the maximum displacement of the punch of $u = 1.8$ cm as well as after unloading the structure. The difference between the two types of composite sheets becomes clearly visible looking at the zoomed area. In the Bondal®N/M case a shearing motion of the face sheets against each other can be observed and the sheet stays straight outside the direct die region. For the Bondal®H case almost no shearing of the face sheets against each other is visible but the sheet becomes definitely more curved over a wide area besides the die location.

Load–deflection curves for the different element versions are given in Figs. 16 and 17. For Bondal®N/M material almost no

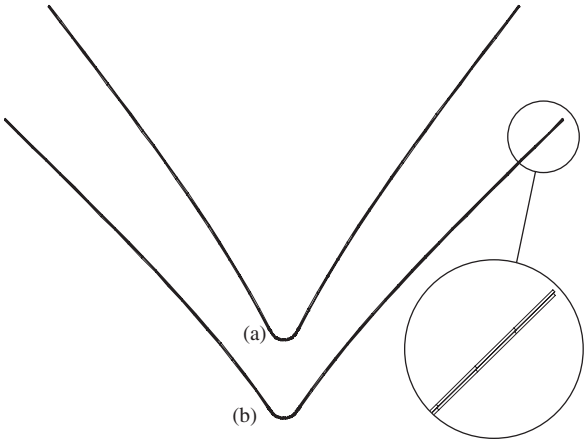

Fig. 14. Composite sheet for free bending experiment (Bondal®N/M); deformed mesh: (a) for $u = 1.8$ cm and (b) after unloading.

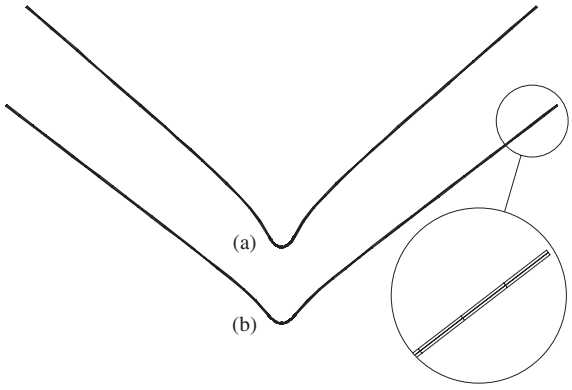

Fig. 15. Composite sheet for free bending experiment (Bondal®H); deformed mesh: (a) at $u = 1.8$ cm and (b) after unloading.

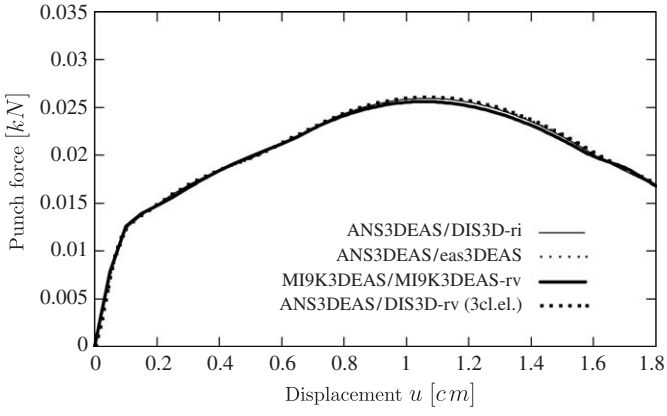

Fig. 16. Load–deflection curves for free bending investigation; Bondal®N/M; comparison of different element combinations (face layer/core layer discretization).

differences are visible between the curves using the bilinear ANS element for the face sheet in combination with the reduced integrated trilinear displacement element for the core sheet (ANS3DEAS/DIS3D-ri), the combination with the EAS element (ANS3DEAS/eas3DEAS), the biquadratic MI9K3DEAS

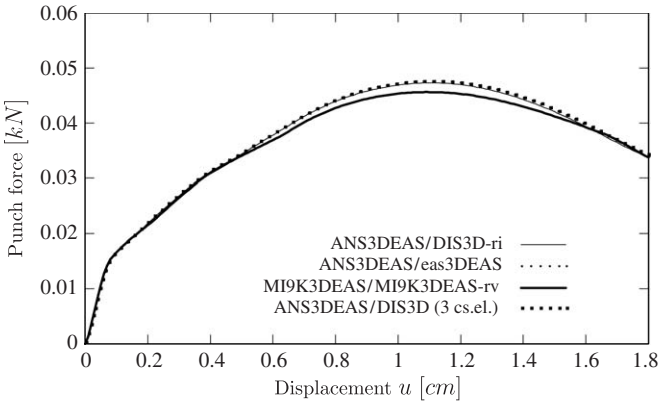

Fig. 17. Load–deflection curves for free bending investigation; Bondal®H; comparison of different element combinations (face layer/core layer discretization).

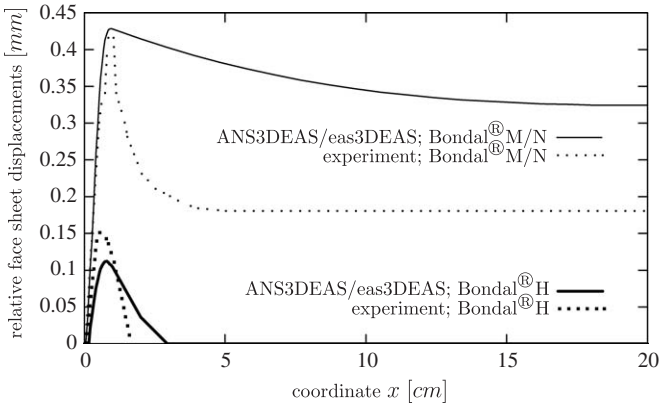

Fig. 18. Relative tangential face sheet displacements for $u = 1.8$ cm along sheet.

element with the selective reduced integrated MI9K3DEAS-rv for the core layer and the combination ANS3DEAS/DIS3D-rv with three elements in thickness direction for the core layer. Comparable results are obtained for Bondal®H. As no experimental results are available for these quantities we can only conclude that the quadratic element appears to lead to the best solutions (Figs. 16 and 17).

In Fig. 18 the relative tangential or shearing displacements of the face sheets for Bondal®N/M as well as for Bondal®H are depicted over the coordinate x for a punch displacement of $u = 1.8$ cm. In the numerical model the relative displacements are fairly large for Bondal®N/M and are barely decreasing outside the die. The experiments show the same maximum displacement, however, the decrease is considerably larger than in the analysis. This difference can be explained with deficits in the knowledge about the material parameters for the core layer. For Bondal®H the relative displacement is much smaller inside the edges of the die and decreases completely outside the die. This result is qualitatively rather close to the experimentally determined results [36].

After finishing the forming process an eigenfrequency analysis is performed for the deformed structure to investigate

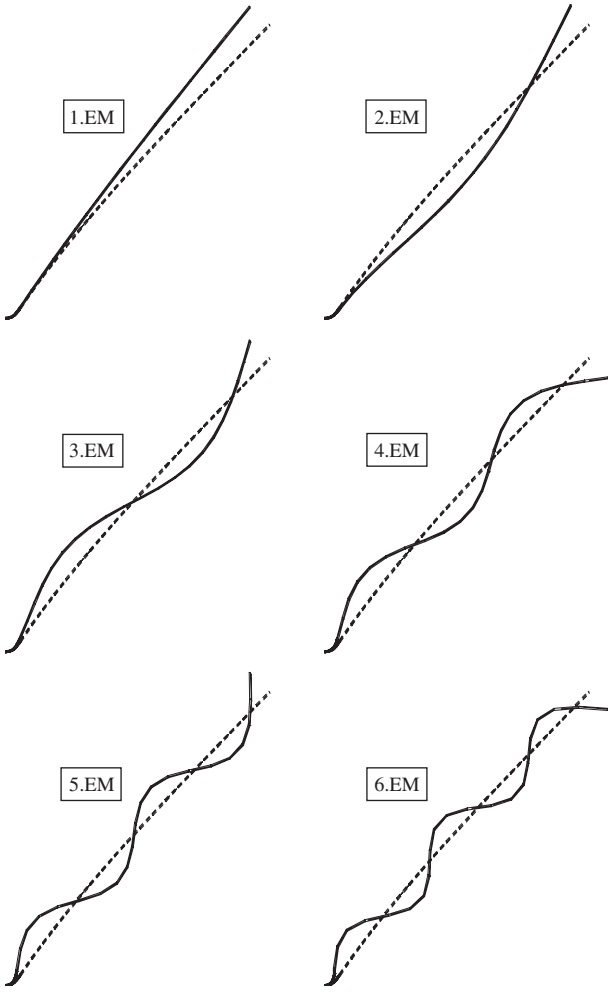

Fig. 19. Free bending experiment; Bondal®N/M; deformed geometry and eigenmodes (EM) 1.0–6.0, taking residual stresses into account.

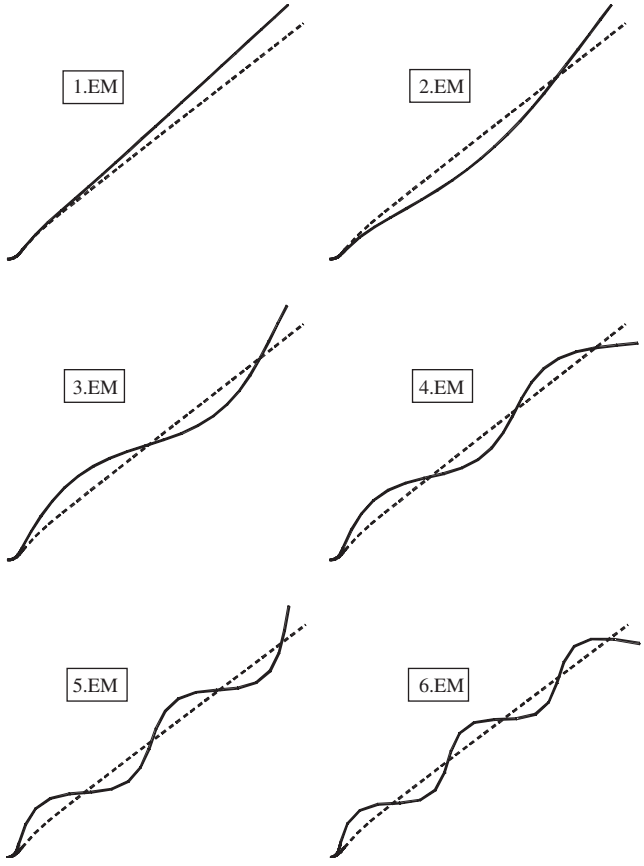

Fig. 20. Free bending experiment; Bondal®H; deformed geometry and eigenmodes (EM) 1.0–6.0, taking residual stresses into account.

the forming effects on the eigenfrequencies thus the acoustic properties. Within the simulation the work piece is unloaded by reducing the contact forces iteratively down to zero. For the unloaded deformed structure the eigenmodes and eigenfrequencies are computed. These results are compared with the eigenfrequencies of a geometrically identical workpiece which is free of any residual stresses. The eigenmodes for the formed pieces including residual stresses are shown in Figs. 19 and 20 for the first six eigenfrequencies. The associated eigenfrequencies are given in Table 8. Comparing the eigenfrequencies for the formed structure with residual stresses and for the structure without residual stresses in the Bondal®N/M case only for the first rather low frequency a clear difference is found in contrast to the Bondal®H case where clear differences between all frequencies are visible. The reason for this clearly different behavior of the two types of composite sheets is definitely due to the different material properties of the core layers and the shear stresses inside the core layer.

Comparing the material properties of Bondal®N/M with Bondal®H it is obvious that the stiffness of the Bondal®N/M is smaller but the yield stress is much higher than for the Bondal®H. After unloading the formed structure transverse shear stresses remain inside the core layer. For Bondal®N/M these stresses are smaller in the core layer, though the relative displacements are considerably large and the stiffness of the core layer has little influence on the global stiffness. Thus there is almost no difference to the stiffness of the unloaded structure. As a consequence no influence on the vibration properties can be expected. For Bondal®H the residual shear stresses are larger and some plastic deformation of the core layer material has taken place. In addition the strains are in the plastic range. Therefore, smaller eigenfrequencies for the blank, where the loading history has been taken into account, have to be expected. Thus, obviously the influence of the loading history of the forming process has to be taken into account, if the vibration properties have to be investigated.

4.3. Deep drawing of composite sheet with analysis of eigenfrequencies

In this section the deep drawing process for a pasted composite sheet with the geometric properties are given in Fig. 21 is investigated. The total thickness of the sheet is $t = 1$ mm with a core layer thickness of 0.04 mm representing the glue and two metal face sheets of 0.48 mm thickness each. The rigid forming tools are a cylindrical punch with radius $R_p = 2$ cm, plane blank

Table 8
Eigenfrequencies for eigenmodes (EM) 1.0–6.0 for composite sheet; free bending experiment; comparing influence of residual stresses for both core layer materials

	Bondal®N/M		Bondal®H	
	After unloading with residual stresses	Directly generated without residual stresses	After unloading with residual stresses	Directly generated without residual stresses
1.EM	4.04×10^{-2}	4.62×10^{-2}	1.26×10^{-1}	1.63×10^{-1}
2.EM	1.65×10^{0}	1.70×10^{0}	3.30×10^{0}	3.78×10^{0}
3.EM	1.31×10^{1}	1.33×10^{1}	1.89×10^{1}	2.17×10^{1}
4.EM	5.10×10^{1}	5.15×10^{1}	5.92×10^{1}	6.89×10^{1}
5.EM	1.42×10^{2}	1.42×10^{2}	1.46×10^{2}	1.72×10^{2}
6.EM	3.21×10^{2}	3.22×10^{2}	2.94×10^{2}	3.68×10^{2}

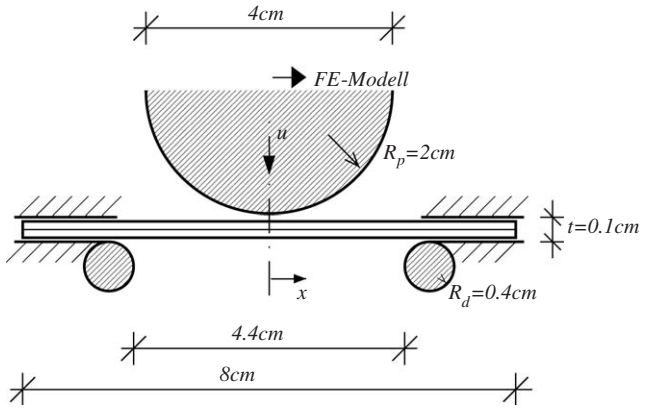

Fig. 21. Geometry properties for deep drawing process of composite sheet.

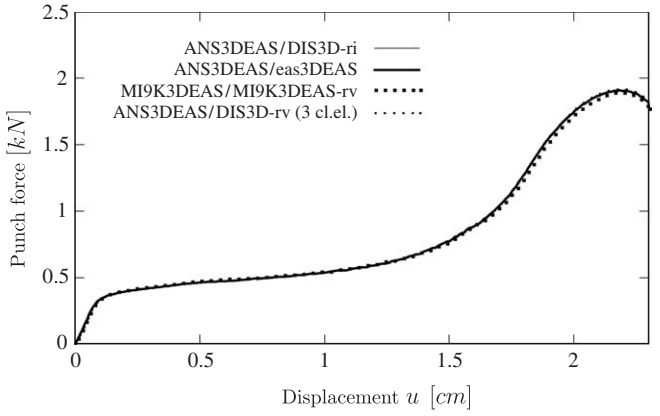

Fig. 22. Load–deflection curves for deep drawing process of composite sheet; Bondal®N/M; comparison of different element combinations (face layer/core layer discretization).

holders with a die radius $R_d = 0.4$ cm at the edges. A uniform discretization of the sheet with 100 bilinear and 50 biquadratic solid-shell elements in longitudinal direction is chosen. Due to symmetry only half of the model is considered. The satisfaction of the contact condition is checked directly at the contact integration points, the so-called local approach of contact integration, with two Gauss points for the bilinear and three for the biquadratic contact surfaces, see e.g. [12].

As such composite sheets are primarily used to influence acoustic emissions in dynamically loaded structures, a further focus is on the effect of forming on the eigenfrequencies. This may be important for a proper analysis of the correct eigenfrequencies.

In Fig. 22 the load–deflection curves for the Bondal®N/M composite sheet are shown with the punch force vs. the displacement u at the center of the die. For the three model versions using bilinear elements for core and face layer discretization the curves are almost identical. Only the combination MI9K3DEAS/MI9K3DEAS-rv is slightly softer for $u > 1.5$ cm.

For Bondal®H (see Fig. 23) the combination MI9K3DEAS/MI9K3DEAS-rv is again slightly softer compared to the combination ANS3DEAS/DIS3D-ri for $u > 1.5$ cm. Remarkably the combination ANS3DEAS/eas3DEAS shows an artificial oscillation behavior for $u > 1.8$ cm. Additional tests with the element stabilization discussed in Section 3.1 by switching off critical element modifications reveal that this behavior is caused by the

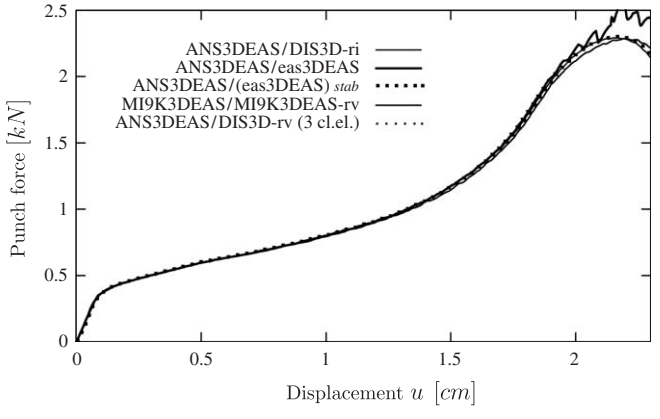

Fig. 23. Load–deflection curves for deep drawing process of composite sheet; Bondal®H; comparison of different element combinations (face layer/core layer discretization).

ANS modification which obviously leads in combination with the six parameter enhancement of the membrane strains to artificial kinematics. Stabilizing the core layer elements by switching off the ANS modification (ANS3DEAS/$(\text{eas3DEAS})_{\text{stab}}$) leads to a curve identical to the ANS3DEAS/DIS3D-ri combination.

In Figs. 24 and 25 the deformed meshes for Bondal®N/M and Bondal®H are shown for the maximum displacement $u = 2.3$ cm of the die and after unloading. The unloading is done by setting the contact forces stepwise to zero and iteratively solving the nonlinear equations. In both cases the work pieces change their shape during the unloading process (springback) especially for Bondal®H, as it is well known for high strength steels. Therefore, it is definitely necessary to take the unloading process into account and the residual stresses in the numerical forming simulation to get the final correct geometry of the workpiece.

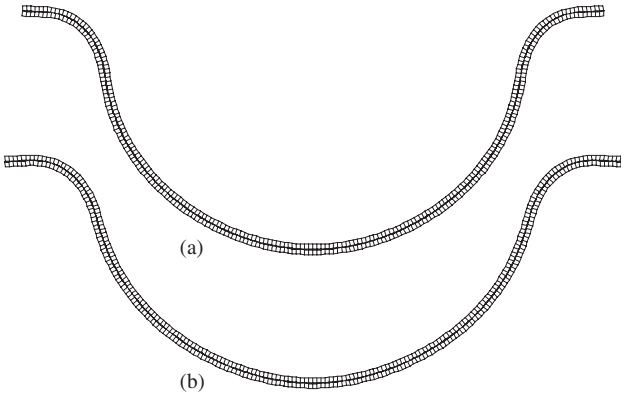

Fig. 24. Deep drawing of composite sheet Bondal®N/M; deformed mesh: (a) at $u = 2.3$ cm and (b) after unloading.

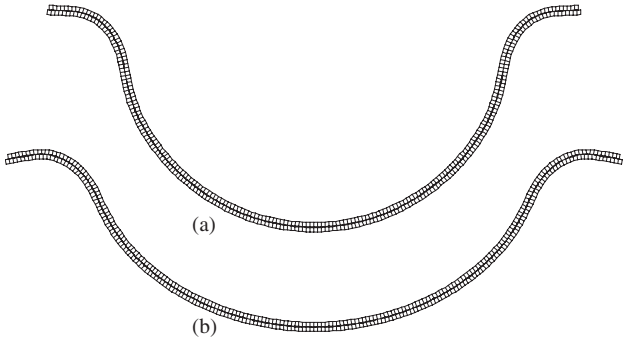

Fig. 25. Deep drawing of composite sheet Bondal®H; deformed mesh: (a) at $u = 2.3$ cm and (b) after unloading.

After unloading the eigenmodes and eigenfrequencies of the deformed composite sheet are computed. To compare the results also a model with the identical geometry but without residual stresses and strains is investigated. This is done with respect to a proper investigation of the acoustic properties of structures made of composite sheets. The eigenfrequencies are given in Table 9, the eigenmodes are depicted in Figs. 26 and 27. Again only for the Bondal®H major differences are visible between

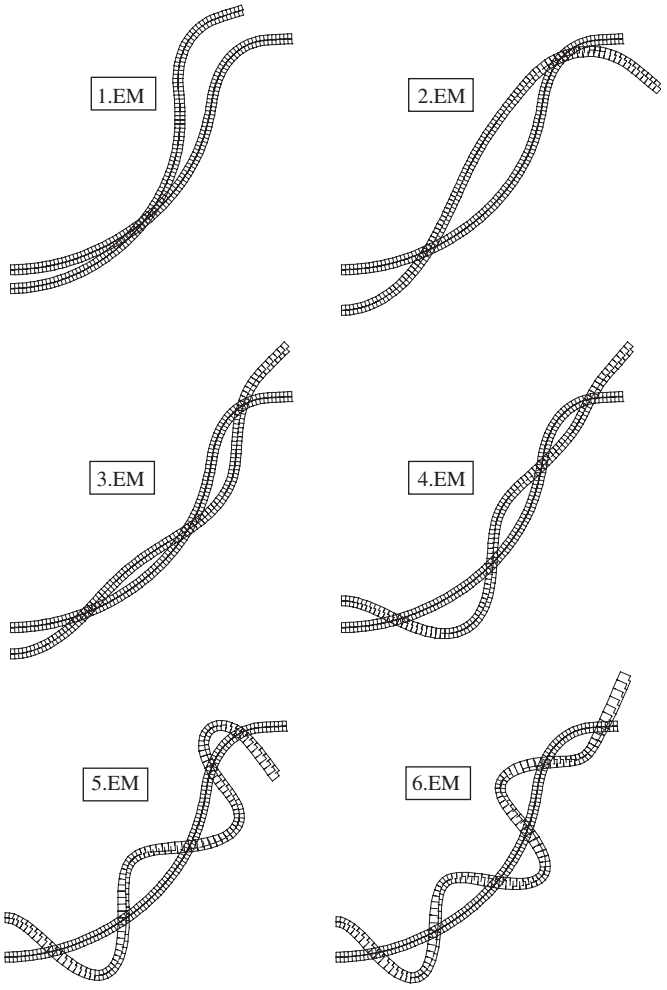

Fig. 26. Deep drawing of composite sheet; Bondal®N/M; Eigenmodes (EM) 1.0–6.0 and deformed geometry.

Table 9
Eigenfrequencies (EV) for eigenmodes 1.0–6.0 for deep drawn composite sheet; comparing influence of residual stresses for both core layer materials

	Bondal®N/M		Bondal®H	
	After unloading with residual stresses	Directly generated without residual stresses	After unloading with residual stresses	Directly generated without residual stresses
1.EV	4.65×10^1	4.61×10^1	4.89×10^1	7.96×10^1
2.EV	1.83×10^3	1.82×10^3	9.67×10^2	2.09×10^3
3.EV	9.44×10^3	9.42×10^3	4.80×10^3	9.86×10^3
4.EV	3.07×10^4	3.06×10^4	1.38×10^4	3.16×10^4
5.EV	9.11×10^4	9.10×10^4	3.29×10^4	9.27×10^4
6.EV	2.06×10^5	2.06×10^5	7.74×10^4	2.08×10^5

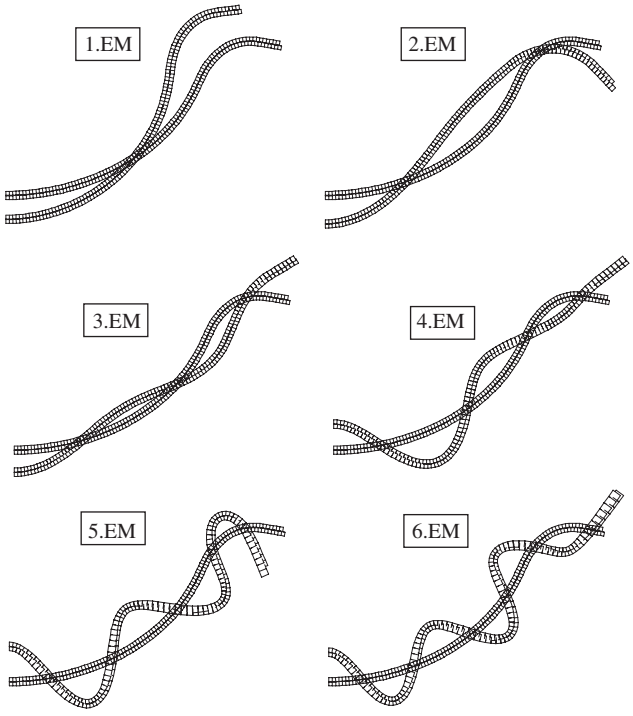

Fig. 27. Deep drawing of composite sheet; Bondal®H; Eigenmodes (EM) 1.0–6.0 and deformed geometry.

the eigenfrequencies of the structure taking into account the deformation process and the residual stresses and those of the model without residual stresses.

As before this behavior is due to the different material properties of the core layer. After unloading the formed blank for the Bondal®N/M shear strains remain in the core layer inside the elastic range of the material whereas for Bondal®H the shear strains are dominantly inside the plastic range of the core layer material. The latter effect results then in a softening effect for the core layer of the Bondal®H case and in smaller eigenfrequencies for the formed blank.

5. Comments on structural and material stability problems

The solid-shell elements introduced in [1,4–6] have been used in many shell stability investigations and nonlinear analyses by the authors, where no hourglass instabilities were encountered. This is due to the fact that hardly highly constrained situations are encountered in shell stability problems. Such situations, however, were expected in sheet metalforming, where some instabilities were found as discussed above.

Within the proposed control scheme the enhanced strain elements are taken as a basis which are well known to allow the detection of material instability effects and in general show superior behavior for such problems. However, the investigations were not including any material instability problems.

6. Conclusions

In the first part of this contribution a short introduction into the solid-shell concept was given. This special kind of shell elements is preferable for some applications as for example in sheet metal forming using layered composite sheets. The necessary modifications to remove locking effects such as approaches of reduced integration and mixed element formulation, are briefly described for the elements used.

For special situations like homogeneous stress states it was observed that the modified elements show artificial kinematics which are due to modifications which are not necessary in this specific case. Therefore, a simple stabilization procedure has been suggested which is based on a check of the loading state and to decide then which modifications are necessary to avoid expected locking effects and which modifications should be better taken out to avoid numerical instabilities. Then the internal energies of the modified and the unmodified element formulations are compared which finally indicates whether a modification leads to a softening effect and therefore prevents some locking effects or not. In the latter case this element modification should not be used. In some small numerical examples it was shown that such a simple procedure for automatically choosing the appropriate element modification is working very well.

In a final section of the paper a special application for solid-shell elements, the numerical treatment of pasted composite sheets, is investigated. First the discretization of the composite sheets—three or more elements are used for discretization in thickness direction—including the problems resulting from this very special discretization using solid-shells even for description for the very thin core layer with material properties much different from those of the metal face sheets are discussed. Finally some numerical examples are presented, describing typical forming processes for the composite sheets. After finishing the numerical simulation of the forming process including the unloading of the structure simulating the so-called springback effect, eigenfrequency analyses have been performed to investigate the influence of residual stresses and plastic straining introduced by the forming process to the dynamic behavior of the structure. The numerical examples show—even for the rather simple geometry—that it is important for certain material combinations to take the deformation process fully into account.

Acknowledgments

The authors thank the Deutsche Forschungsgemeinschaft, Bonn-Bad Godesberg for the support under grant DFG-Schw 307/13-2.

References

[1] R. Hauptmann, K. Schweizerhof, A systematic development of solid-shell element formulations for linear and nonlinear analysis employing only displacement degrees of freedom, Int. J. Numer. Meth. Eng. 42 (1998) 49–70.

[2] H. Schoop, Oberflächenorientierte Schalentheorien endlicher Verschiebungen, Ing. Arch. 56 (1986) 427–437 (in German).

[3] H. Parisch, A continuum-based shell theory for non-linear applications, Int. J. Numer. Meth. Eng. 38 (1995) 1855–1883.

[4] R. Hauptmann, S. Doll, M. Harnau, K. Schweizerhof, 'Solid-Shell' elements with linear and quadratic shape functions at large deformations

with nearly incompressible materials, Comput. Struct. 79 (18) (2001) 1671–1685.
[5] M. Harnau, K. Schweizerhof, About linear and quadratic 'Solid-Shell' elements at large deformations, Comput. Struct. 80 (9–10) (2002) 805–817.
[6] R. Hauptmann, K. Schweizerhof, S. Doll, Extension of the solid-shell concept for large elastic and large elastoplastic deformations, Int. J. Numer. Meth. Eng. 49 (2000) 1121–1141.
[7] M. Harnau, Finite Volumen-Schalenelemente für große Deformationen und Kontakt, Dissertation, Institut für Mechanik, Universität Karlsruhe, 2004 (in German).
[8] L. Vu-Quoc, X.G. Tan, Optimal solid shells for nonlinear analyses of multilayer composites. Part I: statics, Comput. Meth. Appl. Mech. Eng. 192 (2003) 975–1016.
[9] L. Vu-Quoc, X.G. Tan, Optimal solid shells for nonlinear analyses of multilayer composites. Part II: dynamics, Comput. Meth. Appl. Mech. Eng. 192 (2003) 1017–1059.
[10] X.G. Tan, L. Vu-Quoc, Efficient and accurate multilayer solid-shell element: nonlinear materials at finite strain, Int. J. Numer. Meth. Eng. 63 (15) (2005) 2124–2170.
[11] X.G. Tan, L. Vu-Quoc, Optimal solid shell element for large-deformable composite structures with piezoelectric layers and active vibration control, Int. J. Numer. Meth. Eng. 64 (15) (2005) 1981–2013.
[12] M. Harnau, A. Konyukhov, K. Schweizerhof, Algorithmic aspects in large deformation contact analysis using 'Solid-Shell' elements, Comput. Struct. 83 (21–22) (2005) 1804–1823.
[13] P. Wriggers, S. Reese, A note on enhanced strain methods for large deformations, Comput. Meth. Appl. Mech. Eng. 135 (1996) 201–209.
[14] M. Bischoff, Theorie und Numerik einer dreidimensionalen Schalenformulierung, Dissertation, Report No. 30, Institut für Baustatik, Universität Stuttgart, 1999 (in German).
[15] M. Bischoff, E. Ramm, Shear deformable shell elements for large strains and rotations, Int. J. Numer. Meth. Eng. 40 (1997) 4427–4449.
[16] C. Miehe, A theoretical and computational model for isotropic elastoplastic stress analysis in shells at large strains, Comput. Meth. Appl. Mech. Eng. 155 (1998) 193–234.
[17] B. Seifert, Zur Theorie und Numerik finiter elastoplastischer Deformationen von Schalenstrukturen, Dissertation, Report No. F 96/2, Institut für Baumechanik und Numerische Mechanik, Universität Hannover, 1996 (in German).
[18] R.J. Alves de Sousa, R.M. Natal Jorge, R.A. Fontes Valente, J.M.A. Cesar de Sa, A new volumetric and shear locking-free 3D enhanced strain element, Eng. Comput. 20 (2003) 896–925.
[19] R.A. Fontes Valente, R.J. Alves de Sousa, R.M. Natal Jorge, An enhanced strain 3D element for large deformation elasto-plastic thin-shell applications, Comput. Mech. 34 (2004) 38–52.
[20] R.J. Alves de Sousa, R.P.R. Cardoso, R.A. Fontes Valente, J.W. Yoon, R.M. Natal Jorge, J.J. Gracio, A new one-point quadrature EAS solid-shell element accounting for multi-points along thickness. Part I—geometrically linear problems, Int. J. Numer. Meth. Eng. 62 (2005) 952–977.
[21] K.D. Kim, G.Z. Liu, S.C. Han, A resultant 8-node solid-shell element for geometrically nonlinear analysis, Comput. Mech. 35 (5) (2005) 315–331.
[22] J.C. Simo, F. Armero, Geometrically non-linear enhanced strain mixed methods and the method of incompatible modes, Int. J. Numer. Meth. Eng. 33 (1992) 1413–1449.
[23] E. Dvorkin, K.J. Bathe, A continuum mechanics based four-node shell element for general nonlinear analysis, Eng. Comput. 1 (1984) 77–88.
[24] E.N. Bucalem, K.J. Bathe, Higher-order MITC general shell elements, Int. J. Numer. Meth. Eng. 36 (1993) 3729–3754.
[25] N. Büchter, E. Ramm, D. Roehl, Three-dimensional extension of non-linear shell formulation based on the enhanced assumed strain concept, Int. J. Numer. Meth. Eng. 37 (1994) 2551–2568.
[26] S. Glaser, F. Armero, On the formulation of enhanced strain finite elements in finite deformations, Eng. Comput. 14 (7) (1997) 759–791.
[27] E.A. de Souza Neto, D. Peric, G.C. Huang, D.R.J. Owen, Remarks on the stability of enhanced strain elements in finite elasticity and elastoplasticity, in: D.R.J. Owen, E. Onate, E. Hinton (Eds.), Computational Plasticity—Fundamentals and Applications. Part I, Pineridge Press, Swansea, 1995.
[28] W.A. Wall, M. Bischoff, E. Ramm, A deformation dependent stabilization technique, exemplified by EAS elements at large strains, Comput. Meth. Appl. Mech. Eng. 188 (2000) 859–871.
[29] J. Korelc, P. Wriggers, Consistent gradient formulation for a stable enhanced strain method for large deformations, Eng. Comput. 13 (1996) 103–123.
[30] S. Reese, M. Kuessner, B.D. Reddy, A new stabilization technique for finite elements in non-linear elasticity, Int. J. Numer. Meth. Eng. 44 (1999) 1617–1652.
[31] S. Reese, P. Wriggers, A stabilization technique to avoid hourglassing in finite elasticity, Int. J. Numer. Meth. Eng. 48 (2000) 79–109.
[32] S. Reese, On a consistent hourglass stabilization technique to treat large inelastic deformations and thermo-mechanical coupling in plane strain problems, Int. J. Numer. Meth. Eng. 57 (2003) 1095–1127.
[33] L. Vu-Quoc, J.A. Mora, A class of simple and efficient degenerated shell elements—analysis of global spurious-mode filtering, Comput. Meth. Appl. Mech. Eng. 74 (1989) 117–175.
[34] L. Vu-Quoc, C. Hoff, On a highly robust spurious-mode filtering method for uniformly reduced-integrated shell elements, Int. J. Numer. Meth. Eng. 34 (1992) 209–220.
[35] S. Reese, Thermomechanische Modellierung gummiartiger Polymerstrukturen. Habilitation, Report No. F01/4, Institut für Baumechanik und Numerische Mechanik, Universität Hannover, 2001 (in German).
[36] M. Büscher, E.-J. Drewes, E. Finckenstein, L. Keßler, W. Nester, V. Steiniger, H.U. Weigel, Simulation der Umformung von oberflächenveredelten Feinblech-Verbundwerkstoffen, Forschungsbericht Projekt 222, Studiengesellschaft Stahlanwendung e.V., 1995 (in German).
[37] S. Doll, R. Hauptmann, K. Schweizerhof, C. Freischläger, On volumetric locking of low-order solid and solid-shell elements for finite elastoviscoplastic deformations and selective reduced integration, Eng. Comput. 17 (2000) 874–902.
[38] J.C. Simo, Algorithms for static and dynamic multiplicative plasticity that preserve the classical return mapping schemes of the infinitesimal theory, Comput. Meth. Appl. Mech. Eng. 99 (1992) 61–112.
[39] H. Hencky, The elastic behavior of vulcanized rubber, Appl. Mech. (J. Appl. Mech.) 1 (1933) 45–53.